Construction and Building Materials 165 (2018) 45–57

Contents lists available at ScienceDirect

Construction and Building Materials

journal homepage: www.elsevier.com/locate/conbuildmat

Experimental investigation of the size effect of layered roller compacted concrete (RCC) under high-strain-rate loading

Xiao-hua Wang [a], She-rong Zhang [a,b], Chao Wang [a,b,*], Ran Song [a], Chao Shang [a], Xin Fang [a]

[a] School of Civil Engineering, Tianjin University, Tianjin 300072, China
[b] State Key Laboratory of Hydraulic Engineering Simulation and Safety, Tianjin University, Tianjin 300072, China

HIGHLIGHTS

- Dynamic size effects on the properties of RCC material have been investigated.
- Statistical correlation between strain-rate and size effects on RCC is analyzed.
- A modified Weibull size effect law for RCC is proposed considering strain-rate effect.

ARTICLE INFO

Article history:
Received 24 August 2017
Received in revised form 28 December 2017
Accepted 5 January 2018

Keywords:
Roller compacted concrete
High strain rate
Dynamic size effect
Statistical analysis
Split Hopkinson pressure bar

ABSTRACT

The strain rate and specimen size are two main influential factors when measuring the compressive strength of concrete-like materials. Understanding the dynamic size effect of concrete is essential for better analysis and design of concrete structures. However, few systematic laboratory tests have investigated the dynamic size effect in layered roller compacted concrete (RCC) under various levels of high-strain-rate loading. In this study, three sizes of cylindrical RCC specimens with diameters of 50 mm, 75 mm and 100 mm are prepared and tested under high loading rates to directly investigate the size effects. The size dependence and strain rate sensitivity are characterized in terms of the failure pattern, dynamic compressive strength, ultimate strain, maximum strains, and toughness. The dynamic compressive strength increases with increasing specimen size under impact loading, which is opposite to the size effect under static loading. The statistical significance is further investigated in terms of the variation in the dynamic mechanical properties of the RCC material based on analysis of variance (ANOVA). A modified Weibull size effect law, which incorporates both the specimen size and strain rate, is proposed and verified to illustrate the underlying mechanism of the dynamic size effect for the RCC material under impact loading.

1. Introduction

It is well accepted, based on experimental and theoretical investigations, that the mechanical response of concrete-like materials under compression, shear, tension and torsion under quasi-static loading is significantly affected by the specimen size. Generally, a smaller specimen requires higher stress to fracture under quasi-static loading. The mechanism of the concrete size effect law for the quasi-static strength can be classified into three categories: (1) Weakest-link hypothesis [1,2]: larger structures have a larger chance of containing a critical flaw that can cause complete collapse, and the structure will fail as soon as the first critical defect fails; (2) Energetic (deterministic) mechanism [3–6]: two fundamental causes of the size effect in concrete structures are the material heterogeneity and the stress discontinuities at the crack tips, which cause stress redistribution and stored energy release (i.e., strain energy dissipation) during the development of macrocracks; (3) Fractal mechanism [7]: the roughness of the crack surfaces in concrete exhibits inherent fractal characteristics. When the microstructural disorder and self-similar features (i.e., fractality) dominate the damage and fracturing process, the fractal mechanism permits better interpolation of experimental data than the energetic mechanism.

However, when exposed to high-strain-rate loading, concrete-like materials have a higher dynamic compressive strength than their corresponding static compressive strength [8–11]; the fracture energy is also increased [12]. The experiments conducted by Elfahal [13] and theoretical analysis by Qi [14] indicate that the

* Corresponding author at: School of Civil Engineering, Tianjin University, Tianjin 300072, China.
E-mail address: wangchaosg@tju.edu.cn (C. Wang).

https://doi.org/10.1016/j.conbuildmat.2018.01.033
0950-0618/

Nomenclature

f_d	dynamic compressive strength (MPa)
f_c	quasi-static compressive strength (MPa)
$\Delta f_{\dot{\varepsilon}}$	dynamic strength increase from the material strain-rate effect (MPa)
Δf_i	dynamic strength increase from the structural effect (MPa)
A_{s0}	initial cross-sectional area of the specimen (mm^2)
A_s	real-time cross-sectional area of the specimen (mm^2)
H_{s0}	initial thickness area of the specimen (mm)
H_s	real-time thickness area of the specimen (mm)
$\sigma_s(t)$	engineering stress of the specimen (MPa)
$\varepsilon_s(t)$	engineering strain of the specimen (mm/mm)
$\dot{\varepsilon}_s(t)$	engineering strain rate of the specimen (/s)
c_b	wave propagation velocity in the steel bars (m/s)
A_b	cross-sectional area of the steel bars (mm^2)
E_b	elastic modulus of the steel bars (GPa)
$\varepsilon_T(t)$	transmitted strain in the steel bars (mm/mm)
$\varepsilon_R(t)$	reflected strain in the steel bars (mm/mm)
F_0	corresponding critical value at the 5% significance level
P	cumulative probability density of the failure for a specimen
σ	peak strength of the specimen (MPa)
σ_0	scaling value in Weibull distribution concerned with the mean (MPa)
m	shape parameter or Weibull modulus
$\bar{\sigma}$	mean strength (MPa)
s	standard deviation (MPa)
$\Gamma(*)$	gamma function
N	total number of tests
i	current test number
V	volume of the specimen (m^3)
V_0	average volume of each microcrack (m^3)
σ_{th}	threshold strength of the failure for the specimen (MPa)
σ_1	scaling value in the Weibull size effect law (MPa)
$\dot{\varepsilon}_0$	critical strain rate of the specimen (/s)
α	strain-rate correction factor in the modified size effect law

size effect under impact loading is notably different from the well-known static size effect, in which the dynamic strength increases with the increasing sample size (in terms of the diameter) at a similar strain rate. Moreover, larger specimens display a more significant strain-rate effect. As is known to all, the interpretations of the strain-rate effect on material strength clearly include three main aspects: (1) Lateral confinement effect [15–17]: the lateral inertial force from Poisson's effect and end friction can restrict the lateral deformation of the specimens; (2) Evolution of the cracks [10]: cracks can form and propagate in coarse aggregates under impact loading instead of simply initiating and propagating in the interfacial transition zone (ITZ); (3) Viscosity effect [10]: the movement of free water in micro-defects within the concrete results in resistance to crack propagation under dynamic loading. However, the interpretation and application of the dynamic size effect are still unclear, i.e., the mechanism of strength enhancement for larger structures under dynamic loading, and the application of laboratory testing results from small structures to real full-scale structures.

Based on the concept of the size effect from Vliet [18,19], the size effect can be considered a combination of the material size effect caused by material heterogeneity and the structural size effect induced by the boundary and shape of the specimen. Similarly, the dynamic strength enhancement of concrete under high-speed impact loading consists of contributions from the material strain-rate effect (which occurs due to the inherent microstructure and crack propagation in aggregates and is considered part of the material size effect) and the structural effect (which occurs due to the lateral confinement and end friction and is considered part of the structural size effect) [20–22]. Under this view, the dynamic increase factor (DIF) obtained from the experimental tests can be expressed as

$$DIF = f_d/f_c = (f_c + \Delta f_{\dot{\varepsilon}} + \Delta f_i)/f_c \quad (1)$$

where f_d is the dynamic compressive strength; f_c is the quasi-static strength; $\Delta f_{\dot{\varepsilon}}$ is the dynamic strength increment due to the material strain-rate effect; and Δf_i is the dynamic strength increment due to the structural effect [22].

With respect to the material size effect, many types of microstructure analysis have been conducted to further understand the macroscopic failure phenomena occurring under impact loading [23,24]. The size effect in concrete has been investigated using Monte Carlo simulations of mesoscale finite element models in which the random inclusions (aggregates and pores) with the prescribed volume fractions, shapes and size distributions are considered [25]. It has been confirmed that the mesoscale heterogeneity, aggregate volume fraction and porosity should not be ignored in the size effect studies of concrete [1,26,27]. The structural size effect on the compressive strength enhancement of the concrete-like material in split Hopkinson pressure bar (SHPB) tests has gained the attention of many researchers. The factors responsible for the structural effects include the material parameters (i.e., hydrostatic dependence and dilation parameter), specimen geometry (i.e., diameter and aspect ratio), end interface friction and material inertia [28].

Much effort has been devoted to explain the relationship among the strength, strain rate and specimen size in the context of the complex micro-structural hierarchy and finiteness of the crack propagation speed [14,29,30]. Although the material strength enhancement under impact loading has been proven to be size-dependent, the size effect on other dynamic material properties at different strain rates remains unclear. Moreover, the size effect law for concrete-like materials is not fully understood under impact loading, resulting in an urgent need to extend size effect law to the full range of strain rates, applicable to both static and dynamic loadings.

Roller compacted concrete (RCC), as a special type of concrete material, has different mixture from traditional concrete, i.e., less water and more fly ash are used to replace Portland cement. The mechanical properties of RCC show higher discreteness in the vertical direction due to the construction technology of thin-layer pouring and vibration rolling [31]. To investigate the dynamic size effect of the RCC under high-strain-rate loading, the actual construction technology was replicated in the laboratory, and RCC specimens were prepared for SHPB tests. The size effect cannot be decoupled from the inherent scatter of strength [1,32], which necessitates the use of a statistical method to estimate the size effect on the strength of concrete and on the damage/fracture process in general. In total, 101 cylindrical specimens with identical length-to-diameter (L/D) ratios of 0.5 but different diameters

(50 mm, 75 mm and 100 mm) were prepared and successfully tested at various strain rates. Using the experimental results, the exposed size effect on the dynamic mechanical properties is further analyzed and discussed to gain a deeper understanding of the physical mechanisms in the observed dynamic size effect. A strain-rate-dependent size effect law is developed to model the dynamic behavior of geometrically similar specimens.

2. Experimental study

2.1. Materials and specimens

In this investigation, ordinary Portland cement was used to prepare the specimens for the SHPB tests; the selected coarse aggregate was artificial coarse aggregate produced by a local aggregate production system. Comprehensive consideration was taken to design the mixture to experimentally investigate the dynamic size effect, as shown in Table 1. Based on the code for the mix design of hydraulic concrete [33], the water-to-cement ratio was 0.50, and the fly ash content was 60% by mass. The sand ratio was selected as 31% by mass according to the performance of the mixture and expected strength of the final concrete. The maximum aggregate size of the RCC cast in the experimental site was 16 mm to satisfy the requirement of the SHPB tests. Fig. 1 shows the specimen preparation process, which was described in our previous work [31] in detail. The rolling technique of "two static rolling + eight dynamic rolling + two static rolling" was used during material preparation. The paving thickness was 10 cm, and there were five layers in total. After curing, three dimensional drilling cores with diameters of 50 mm, 75 mm and 100 mm (D50 mm, D75 mm, and D100 mm) were drilled and cut into cylinders (Fig. 1e). To minimize the testing errors from the specimens, the surfaces of the cylindrical specimens should be sufficiently smoothly ground (Fig. 1f).

The axial inertia effect can disprove the homogeneity assumption of stress and strain, which is the foundation of the SHPB tests. To minimize the axial inertia effect and reflect the actual dynamic responses of the RCC, the optimal L/D ratio of 0.5 was used to design specimens for the SHPB tests [15]. Grease was also used to minimize the dynamic friction of the specimen-apparatus interfaces; thus, we can reasonably consider the end friction confinement effect to be negligible according to previous studies [16,20]. In order to evaluate the damage level of concrete, it has been confirmed as a useful method to compare the ultrasonic wave velocity measured in situ with that measured on concrete cores [34]. In this study, to minimize the effect of drilling and grinding on the test results, we monitored the damage of the RCC before and after drilling and grinding using ultrasonic wave velocity, and we removed drilling cores with excessive damage. This measurement is quite requisite for the D50mm cores in particular.

2.2. SHPB technology

High-strain-rate impact tests were conducted using the SHPB test system. To avoid oscillation of the stress-strain curves, a half-sine stress waveform was selected as the ideal loading method to perform SHPB tests on quasi-brittle materials. In addition, the incident waves must also have a certain rising time to avoid destroying the sample before the stress balance between the two specimen surfaces. To reduce friction, Vaseline was uniformly daubed on the two specimen/bar contact surfaces. The strikers, which are propelled by the gas gun, impact against the incident bar. In this way, a stress pulse can be generated in the incident bar that spreads towards the specimens. Due to the differential wave impedance between the specimen and the incident bar, part of the stress pulse is transmitted via the specimen as a compressive pulse, and part of stress pulse is reflected into an incident bar as a tensile pulse. The strain gauges mounted on the incident and transmitted bars can record the incident, reflected and transmitted pulses during the entire impact process. Fig. 2 shows the typical stress signals in incident and transmitted bars obtained from an SHPB test. Due to the stress equilibrium requirement during specimen failure, the stress pulse typically must reflect at least 3–4 times before destruction. The one-dimensional wave propagation assumption and the homogeneity assumption of stress and strain for the RCC specimens in SHPB tests were verified in our previous work [31] in detail.

Because it is challenging to accurately measure the real-time cross-sectional area (A_s) and thickness (H_s) of the specimen during the high-speed deformation, we replace them with the initial thickness H_{s0} and cross-sectional area A_{s0} in the calculation of engineering stress-strain curves, which is justified by the fact that the change in specimen thickness and cross-sectional area in SHPB tests is minimal. The "one-wave analysis" method [35] is used to calculate the engineering stress $\sigma_s(t)$, strain $\varepsilon_s(t)$ and strain rate $\dot{\varepsilon}_s(t)$ as follows:

$$\dot{\varepsilon}_s(t) = \frac{2c_b}{H_{s0}}\varepsilon_R \tag{2}$$

$$\varepsilon_s(t) = \frac{2c_b}{H_{s0}}\int_0^t \varepsilon_R(t)dt \tag{3}$$

$$\sigma_s(t) = \frac{A_b E_b}{A_{s0}}\varepsilon_T(t) \tag{4}$$

where c_b is the wave propagation velocity in the steel bars; H_{s0} and A_{s0} denote the original length and cross-sectional area of the specimen, respectively; A_b is the cross-sectional area of the steel bars; and E_b is the elastic modulus of the steel bars. In addition, $\varepsilon_T(t)$ and $\varepsilon_R(t)$ are the transmitted strain and reflected strain, respectively.

2.3. Schematic design

Regarding the dynamic mechanical properties, various cross-sectional strikers or thin copper pulse shapers were used in the tests to achieve the half-sine stress wave loading. By varying the gas pressure of the gas gun (1.5–8 bar) and diameters of the specimens (D50 mm, D75 mm, and D100 mm), we caused specimens with different sizes to undergo various strain rates. The schematic design of the experimental tests is illustrated as Table 2. The specimens prepared for the SHPB tests can be classified into three categories based on the specimen diameter. For each category with identical diameter, the specimens can be divided into four groups based on the gas pressure in the SHPB tests. We prepared 10 specimens for each group (i.e., 120 specimens for the SHPB tests in

Table 1
Mixture proportion for RCC.

W/C	Sand ratio (%)	Fly ash content (%)	Water reducing agent (%)	Air entraining agent (%)	Concrete material consumption (kg/m^3)				
					Water	Cement	Fly ash	Sand	Aggregate
0.50	31	60	0.8	0.05	88	70	106	672	1507

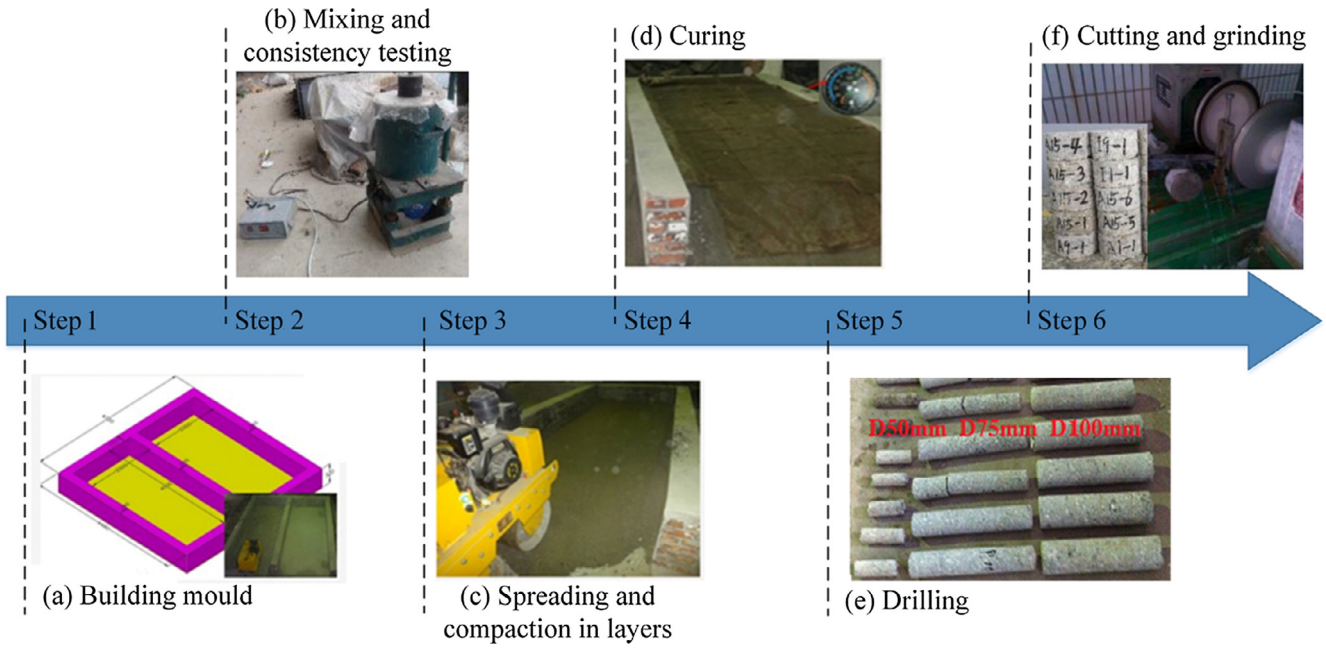

Fig. 1. Specimen preparation process.

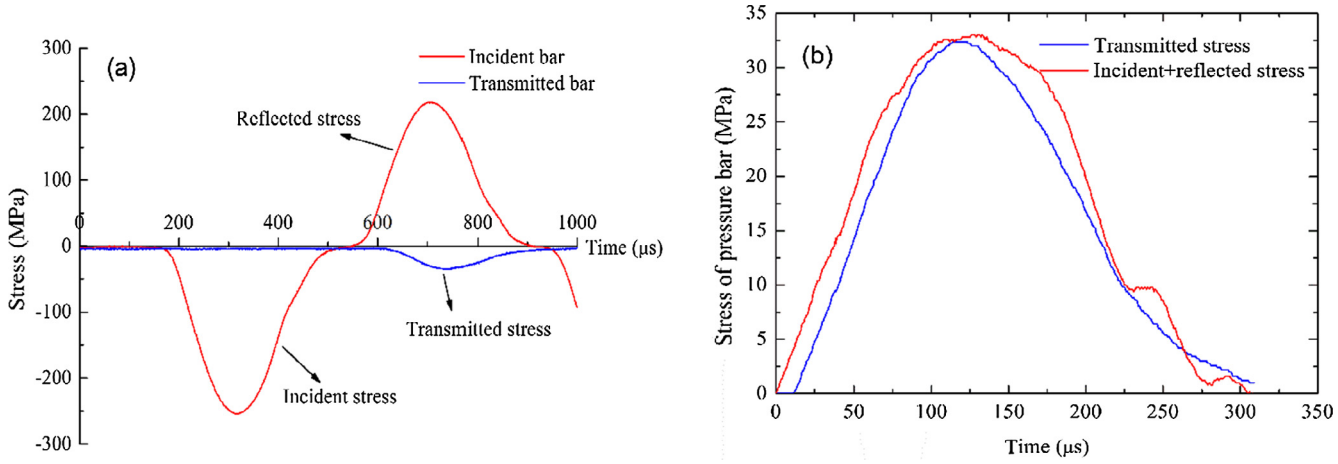

Fig. 2. Typical stress signals: (a) stress in the incident and transmitted bars; (b) achieved stress-equilibrium state.

Table 2
Specimen size and shape for the dynamic loading tests.

Test type	Specimen dimensions (D × L: mm × mm)	L/D	Group	Number	Gas pressure (MPa)	Average strain rate* (/s)
Quasi-static tests (5 cylindrical specimens)	100 × 200	2.0	A	5	–	8.30×10^{-5}
SHPB tests (101 cylindrical specimens)	50 × 25	0.5	D50-A	8	0.30	70.15
			D50-B	8	0.37	88.54
			D50-C	8	0.45	114.45
			D50-D	8	0.55	143.78
	75 × 37.5	0.5	D75-A	7	0.40	46.68
			D75-B	9	0.50	75.84
			D75-C	8	0.60	90.47
			D75-D	8	0.80	111.20
	100 × 50	0.5	D100-A	8	0.15	33.11
			D100-B	10	0.22	47.10
			D100-C	10	0.30	59.83
			D100-D	9	0.37	74.08

* The average strain rate for each group is the mean value of the representative strain rates for the specimens in this group, not the real strain rate for each specimen.

total) at first. However, some specimens for the SHPB tests failed due to incorrect operation or other reasons, and only 101 specimens successfully satisfied the one-dimensional wave propagation assumption and homogeneity assumption of stress and strain. The 101 successfully tested specimens were not uniformly distributed. The specific number for each group has been listed in Table 2.

2.4. Definitions of dynamic mechanical properties

Fig. 3 graphically illustrates the definitions of key mechanical properties in this study: the peak strength, ultimate strain, maximum strain and toughness. The peak value of the stress time history is considered the material strength. The ultimate strain is taken as the strain at peak stress, and the maximum strain of the stress-strain curve is the strain at the end of the softening stage. Moreover, the toughness related to the ductility and strength can be expressed as the specific energy absorption, which is the capacity to absorb the energy of the stress wave for the RCC per unit volume. It is also observed that the material strength occurs nearly at the peak strain rate duration and that the breakage process of the specimen maintains approximately constant strain rate loading since the variation in strain rate with time near the failure point is minimal.

Because the strain rates obtained in the SHPB tests are not constant, the representative strain rate for each specimen can be defined in different ways. However, the strain rate at failure cannot be used to characterize the strain rate during the entire loading process [35], and the mean strain rate, defined as the maximum strain divided by the entire time duration, is notably lower than the instantaneous strain rate at specimen failure [36]. Therefore, the ultimate strain divided by the time duration to reach the peak stress is used as the representative strain rate in this study. Moreover, the mean value of the representative strain rates for specimens in each group is calculated to present the loading condition of this group, denoted as the average strain rate.

3. Experimental results

3.1. Quasi-static testing results

Quasi-static compressive tests on the specimens (diameter × length = 100 mm × 200 mm) were conducted by using an electro-hydraulic servo-controlled loading test machine at Tianjin University. The testing machine delivers a constant crosshead movement with the loading rate of 1 mm/min, corresponding to a quasi-static strain rate of 8.30×10^{-5}/s. The 90 d uniaxial compressive strength of the RCC prepared in this study was 11.13 MPa, and the corresponding Young's modulus and ultimate strain (corresponding to the peak strength) were 2.61 GPa and 0.71%, respectively.

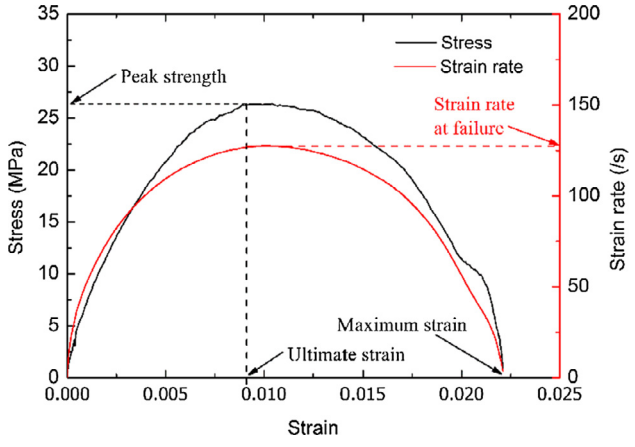

Fig. 3. Diagrammatic sketch of the definitions of the characteristic values in the stress-strain curve.

The quasi-static strength will be used to calculate the dynamic increase factor (DIF) of material strength for RCC material based on the experimental tests. Discussions on strain-rate effect and dynamic size effect in terms of DIFs are given in Section 3.4.

3.2. Dynamic size effect on failure patterns

The RCC specimens with various sizes were prepared and tested under different loading rates by varying the gas gun pressure. The failure patterns at different strain rates, as was concluded in Ref. [31], are notably similar in specimens of different size. Fig. 4 shows the schematic failure patterns of the RCC at various strain rates, which can be summarized as follows. Visible cracks form in the ITZs and propagate along the interfaces under static loading (Fig. 4a). At the critical strain rate, the propagating path becomes straighter, and the fracture surface is less ragged (Fig. 4b). At a high strain rate, the cracks propagate along several direct paths with more fractured aggregates and the specimens ultimately are crushed into several fragments (Fig. 4c). With increasing strain rate, the specimens can be further crushed into finer granularities, which dissipate more energy (Fig. 4d). To sum up, stress increases so rapidly at higher strain rates that the cracks do not have sufficient time to propagate along the path of least resistance and propagate in aggregates instead, resulting in smaller fragments.

Notably, the critical strain rate can be reduced by increasing the specimen size. Therefore, the failure pattern or other dynamic mechanical properties under impact loading may be significantly affected by both strain rate and specimen size. For example, the fracture status of the samples changes from fine fragments to large blocks when the specimen diameter is decreased from 100 mm to 50 mm at a similar strain rate of approximately 70/s in the SHPB tests, as shown in Fig. 4e.

3.3. Dynamic size effect on stress-strain curves

Considering the significant discreteness of the RCC from the construction technology, the stress-strain responses of the RCC material for each group are represented by the means and standard deviations. For the specimens with identical sizes, the stress-strain responses of four groups characterized by different average strain rates are compared in Fig. 5a–c to illustrate the strain-rate effect along with significant discreteness. The average stress-strain responses of the RCC specimens with different sizes share common characteristics: they change significantly with increasing strain rates. The peak stress increases at a higher strain rate, which we refer to as strain-rate dependence resulting from the comprehensive effects of the inertial effect, crack propagation effect and viscosity effect. The slopes of the ascending and descending parts of the stress-strain curves tend to be steeper when the strain rate increases.

The average stress–strain curves for specimens of different dimensions at a similar strain rate (approximately 70/s) are compared in Fig. 5d. A notable change in these curves demonstrates the dynamic size effect. The stress-strain curves of the larger specimens are much steeper than those of smaller specimens, i.e., the peak stress increases when the specimen size increases.

3.4. Dynamic size effect on DIF for compressive strength

Using the D50 specimens as an example, Table 3 summarizes the testing results of dynamic compressive strength and corresponding strain rate for the D50 specimens, which have been classified into four groups according to the gas gun pressure as shown

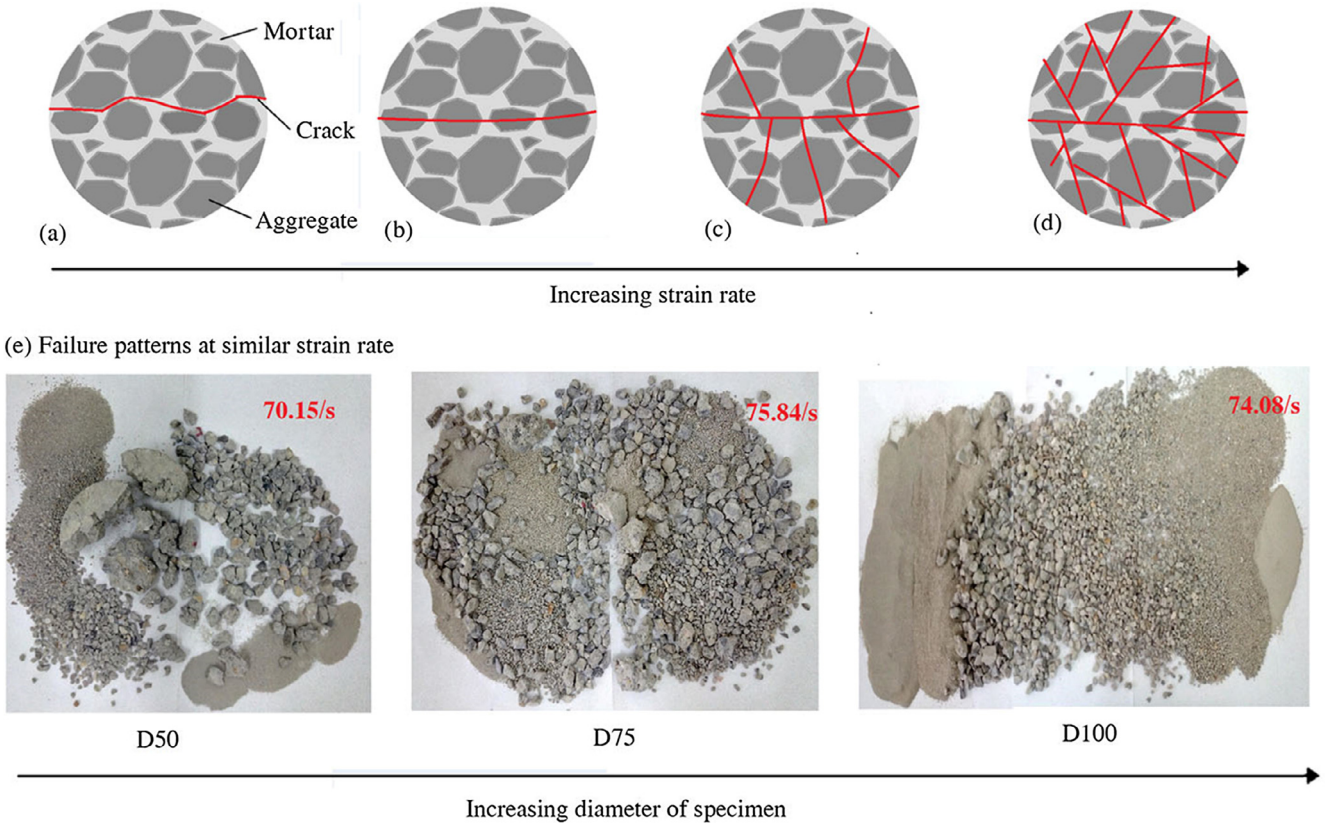

Fig. 4. Failure patterns of the RCC specimens: (a)–(d) schematic failure patterns at various strain rates; (e) failure patterns of specimens with various diameters.

in Table 2. It is obvious from Table 3 that the mean values of dynamic compressive strength for each RCC group increases with the increasing average strain rate. The same rules have been seen in specimens with diameters of 75 mm and 100 mm as well.

Various concrete-like materials have been studied using laboratory tests to quantify the strain-rate effects, and the polynomial fitting method has been widely used to illustrate the empirical relationship between the strain rates and the DIFs [17,35,37–40]. Fig. 6 compares the obtained DIFs with the existing empirical models from other studies. In general, the test results are distributed among these empirical models. Moreover, the DIF increases with increasing strain rate, and the DIFs of the RCC appear more sensitive to the strain rate than the DIFs of normal concrete. Fig. 6 also shows that the DIFs tend to be more sensitive to the strain rate for larger specimens. The test results are consistent with the observations of previous studies [15] that the DIFs obtained from the impacting tests are directly composed of contributions from the inherent strain-rate effect and structural effect. With increasing strain rete, the difference in DIFs among specimens of various dimensions tends to be more significant, which indicates the strain rate sensitivity of the size effect.

3.5. Dynamic size effect on mechanical properties

Fig. 7 compares the experimental results of the dynamic compressive properties, which are represented by the mean values and standard deviations, for specimens with various sizes and strain rates. For specimens with 50 mm in diameter (D50 mm), when the strain rate increases from 70.15 to 143.78/s, the average peak strength continuously increases from 10.08 to 22.28 MPa. The ultimate strain and maximum strain continually increase from 0.0070 to 0.0113 and from 0.0205 to 0.0278, respectively. In addition, the average toughness slightly increases by as much as 0.19 MJ/m^3. The same trend is observed in the D75mm specimens. Immediately after the average strain rate increases from 46.68 to 111.20/s, the average peak strength increases from 10.75 to 36.71 MPa, as much as 241%. In addition, the average ultimate strain consistently increases from 0.0065 to 0.0131. Because of the increasing ductility and strength, the average toughness increases from 0.11 to 0.98 MJ/m^3. The average peak strength of the D100mm specimens increases from 15.31 to 30.44 MPa when the strain rate increases from 33.11/s to 74.08/s, as well as ultimate strain, maximum strains, and toughness all increase with the strain rate.

All experimental results of the dynamic mechanical properties for the RCC material share significant variability at different strain rates. Moreover, the experimental results suggest that the specimen size is another key factor for the increase in dynamic mechanical properties, e.g., the peak strength, ultimate strain and toughness, as shown in Fig. 7. When the specimen size is larger, the lateral inertia confinement becomes more significant, which ultimately leads to a higher peak strength. For example, the testing results of different dimensional specimens at a similar strain rate (approximately 70/s) show that when the diameter of the specimen increases from 50 mm to 75 mm to 100 mm, the average peak strength monotonically increases from 10.08 MPa to 20.33 MPa to 30.44 MPa. This phenomenon is more prominent in Fig. 7a. Similar trends are observed for other dynamic mechanical properties, such as the ultimate strain and toughness. For the ductility, the maximum strain increases with increasing strain rate for same-size specimens, whereas the size dependence of the maximum strain is indistinct for specimens at a similar strain rate. This phenomenon is graphically illustrated in Fig. 5d. Because of the increasing ductility and strength, the specimens at a high strain rate exhibit a greater toughness than those at a relative low strain rate.

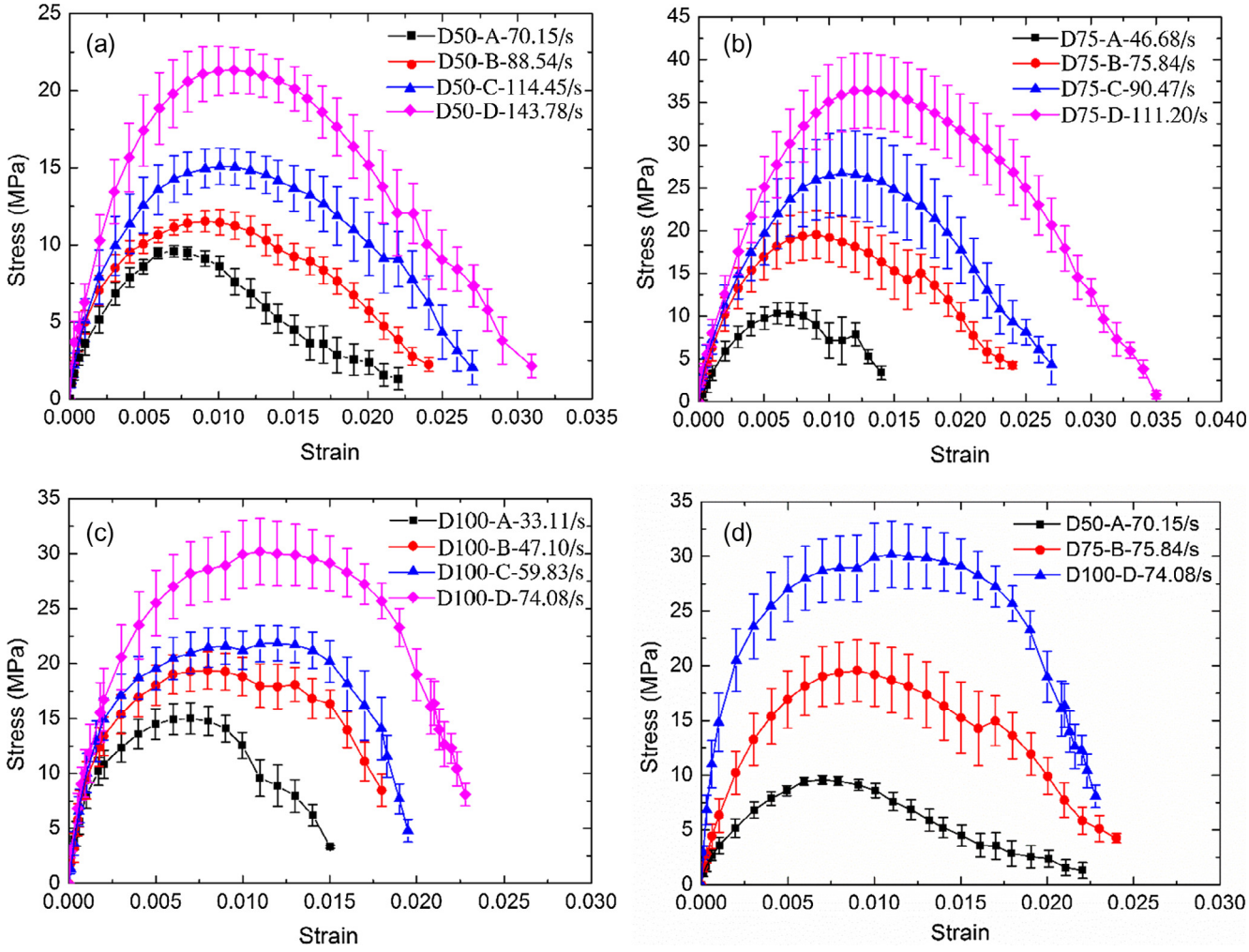

Fig. 5. Average stress-strain curves of the RCC specimens at various strain rates: (a)–(c) for specimens D50, D75, and D100; (d) for specimens of various dimensions at similar strain rates (approximately 70/s).

Table 3
Dynamic compressive strength of D50 RCC specimens (D × L: 50 mm × 25 mm).

Group	Indexes	Testing results								
		Test 1	Test 2	Test 3	Test 4	Test 5	Test 6	Test 7	Test 8	Average
D50-A	Strain rate (/s)	64.27	69.26	70.58	69.28	70.95	71.51	74.31	71.01	70.15
	Strength (MPa)	12.32	8.59	9.12	10.44	8.57	10.74	9.94	10.92	10.08
D50-B	Strain rate (/s)	80.75	98.75	89.75	94.25	92.00	81.68	86.84	84.26	88.54
	Strength (MPa)	12.17	13.36	10.74	12.05	11.51	13.96	12.36	10.21	12.05
D50-C	Strain rate (/s)	111.43	106.10	105.29	123.35	106.36	124.15	123.23	115.72	114.45
	Strength (MPa)	15.30	16.64	18.65	17.11	17.83	15.66	12.59	17.22	16.38
D50-D	Strain rate (/s)	139.45	140.46	143.38	145.75	145.44	142.09	144.68	148.95	143.78
	Strength (MPa)	17.23	23.33	22.32	21.19	22.09	19.17	25.43	27.47	22.28

4. Analysis and discussion

4.1. Analysis of variance (ANOVA)

To further investigate the statistical significance of the strain-rate sensitivity and size dependence on the dynamic mechanical parameters of RCC at high strain rates, the widely accepted method of ANOVA was performed [41]. The F-distribution was used in the ANOVA to evaluate the equality of three or more populations. F_0 is defined as the ratio of two mean squares to estimate whether the null hypothesis can be rejected. In this study, referring to the F-distribution table, the critical value (F_0) can be taken as $F_{0.05,3,28} = 2.95$, representing the critical value with corresponding DOFs of 3 and 28 at a 5% significance level. Therefore, the null hypothesis ($\mu_1 = \mu_2 = \mu_3 = \mu_4$) (i.e., the strain rate has no effect on the dynamic mechanical properties) can be rejected if the P-value is smaller than 0.05 or $F_0 > 2.95$.

Table 4 summarizes all ANOVA results of specimens of various dimensions for the RCC material. The peak strength, maximum strain, and toughness can be significantly affected by the strain

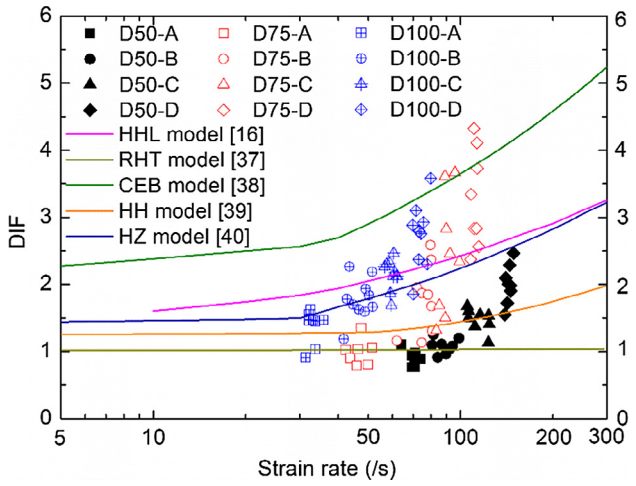

Fig. 6. Comparison of the DIFs from the laboratory tests with that of existing empirical models.

rates for specimens of different dimensions. A smaller P-value provides stronger justification to reject the null hypothesis. The strain-rate effect is notable for almost all of the dynamic mechanical properties, whereas the ultimate strain for the D100 mm specimens is less sensitive to the strain rates. The size effect is detectable for most of the dynamic mechanical properties, apart from the maximum strain. The P-value of the maximum strain, recorded as 0.30 > 0.05, indicates that specimens of different sizes have similar maximum strains. Thus, the size dependence of the maximum strain for the RCC is insignificant.

4.2. Weibull analysis

Zhang [31] suggested that experimental results of the dynamic mechanical properties for RCC share more significant discreteness than that of normal concrete, particularly in the vertical direction, as a result of different mix proportions and construction techniques. Therefore, it is necessary to address the discreteness of the peak strength for the specimens of different dimensions. The weakest-link assumption based on Weibull statistics has been widely used to describe the scatter of material strengths, i.e., that the strength of a structure depends on the weakest volume element [19,32,42]. The Weibull analysis is used with a two-parameter form in the present study, as shown in Eq. (5). In addition, by taking the logarithm twice, the Weibull distribution can be rewritten in linear form as Eq. (6).

$$P(\sigma) = 1 - \exp\left[-\left(\frac{\sigma}{\sigma_0}\right)^m\right] \tag{5}$$

$$\ln[-\ln(1-P)] = m(\ln\sigma - \ln\sigma_0) \tag{6}$$

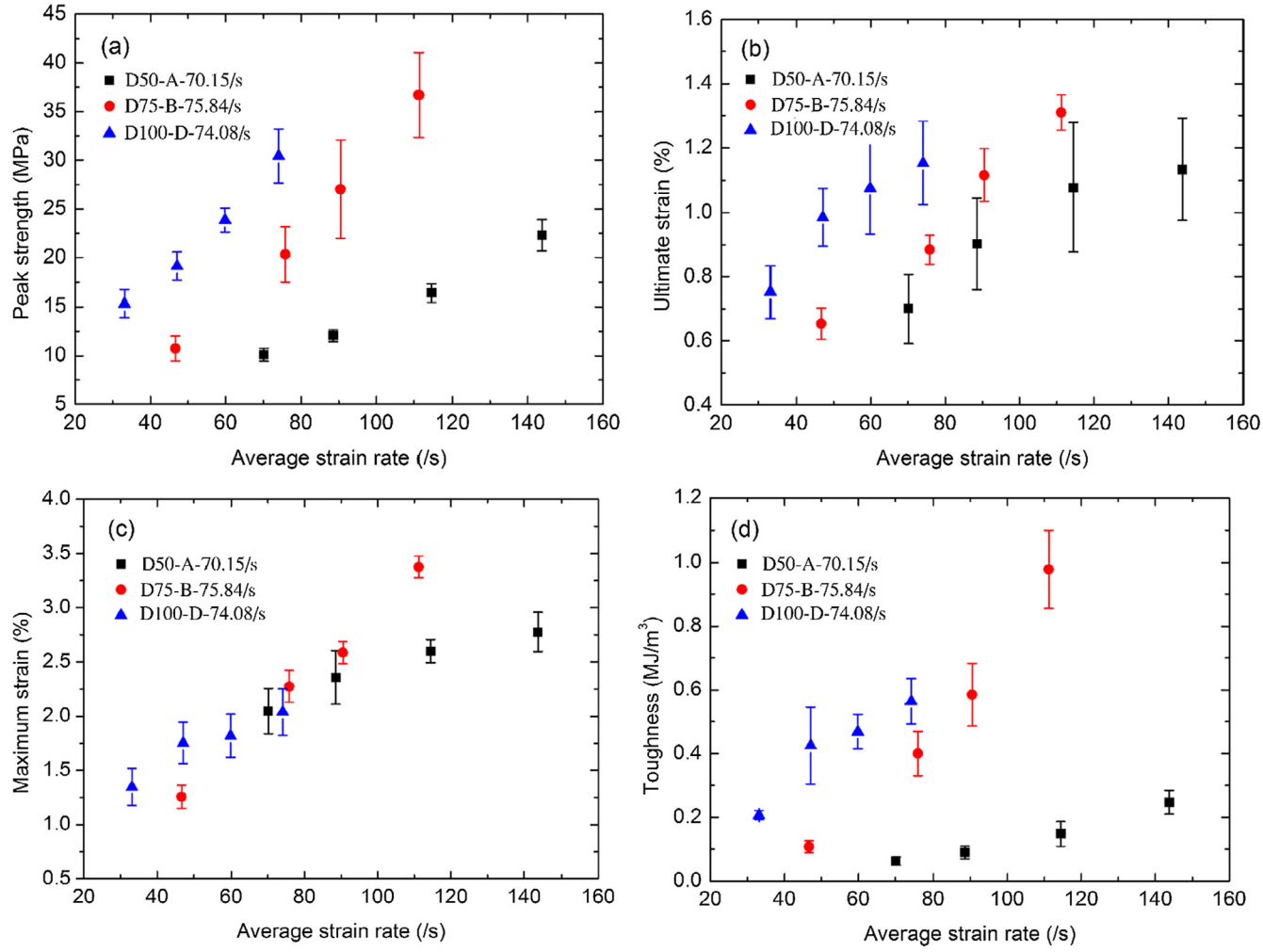

Fig. 7. Dynamic mechanical properties of the RCC specimens at various strain rates: (a) peak strength; (b) ultimate strain; (c) maximum strain; (d) toughness.

Table 4
Summary of the ANOVA for the strain-rate effect and size effect of the RCC.

Property	Strain-rate effect						Size effect	
	D50		D75		D100		Approximately 70/s	
	F_0	P-value	F_0	P-value	F_0	P-value	F_0	P-value
Peak strength	53.80	9.58×10^{-12}	16.84	1.91×10^{-6}	13.76	5.47×10^{-6}	39.37	3.74×10^{-8}
Ultimate strain	5.12	6.00×10^{-3}	48.69	3.10×10^{-11}	0.90	0.45	16.77	3.21×10^{-5}
Maximum strain	5.39	4.70×10^{-3}	109.30	1.45×10^{-15}	4.59	8.60×10^{-6}	1.27	0.30
Toughness	11.94	5.55×10^{-5}	33.55	2.07×10^{-9}	7.86	4.32×10^{-4}	25.41	3.22×10^{-6}

where σ is the peak strength, σ_0 is the scaling value concerned with the mean, and m is the shape parameter or Weibull modulus. Then, the mean and standard deviation can be derived as follows:

$$\bar{\sigma} = \sigma_0 \Gamma\left(1 + \frac{1}{m}\right) \tag{7}$$

$$s = \sigma_0 \sqrt{\Gamma\left(1 + \frac{2}{m}\right) - \Gamma^2\left(1 + \frac{1}{m}\right)} \tag{8}$$

where $\bar{\sigma}$ is the mean strength, s is the standard deviation, and $\Gamma(*)$ is the gamma function.

The cumulative probability density P can be estimated as

$$P = \frac{i}{N+1} \tag{9}$$

where N is the total number of tests and i is the current test number.

The cumulative distribution plots of the experimental results show satisfactory qualitative agreement. Fig. 8 compares the fitted cumulative distribution functions (CDFs) for each group in Table 2, and the Weibull distribution is shown to accurately describe the discrete material strength. Fig. 8 also shows that the fitted cumulative probability curve shifts toward a higher stress value when the strain rate increases for same-size specimens, which indicates a positive effect of the strain rate on material strength. However, the peak strength shows more significant discreteness at higher strain rates since the fitted cumulative probability curve tends to be less steep. Table 5 summarizes the calculated parameters of the fitted Weibull distributions. For the dynamic experimental data, σ_0 increases with increasing strain rate for same-size specimens. However, the statistical results show that the strain-rate effect on the shape parameter is not pronounced, without notable increasing or decreasing trend as the strain rate increases, which indicates an approximately uniform distribution at the selected strain rates. The average shape parameters for the D50 mm, D75 mm, and D100 mm specimens are 10.15, 4.28, and 8.07, respectively, indicating no strong relationship with the specimen size. Table 5 also shows the effect of the strain rate and specimen size on the mean strength ($\bar{\sigma}$) and standard deviation (s). Both the mean strength and standard deviation increase somewhat with increasing strain rate and specimen size.

Fig. 9 graphically presents the mean and standard deviation of strength from Weibull analysis. Relative to the results shown in Fig. 7a, the means and standard deviations of strength derived from the Weibull distribution are notably near to those of the experimental data. Based on the analysis results in this study, empirical formulae in terms of the dynamic compressive strength for the RCC material under impact loading are suggested as follows:

$$\bar{\sigma} = [8.36(\lg \dot{\varepsilon})^2 - 29.94(\lg \dot{\varepsilon}) + 27.70] f_c, \quad \text{for D50 specimens at } 70/\text{s} < \dot{\varepsilon} < 150/\text{s} \tag{10}$$

$$\bar{\sigma} = [13.67(\lg \dot{\varepsilon})^2 - 44.57(\lg \dot{\varepsilon}) + 37.26] f_c, \quad \text{for D75 specimens at } 40/\text{s} < \dot{\varepsilon} < 120/\text{s} \tag{11}$$

$$\bar{\sigma} = [8.59(\lg \dot{\varepsilon})^2 - 25.26(\lg \dot{\varepsilon}) + 19.93] f_c, \quad \text{for D100 specimens at } 30/\text{s} < \dot{\varepsilon} < 80/\text{s} \tag{12}$$

In this study, the dynamic compressive strength increases with increasing specimen size in the condition of identical strain rates, which is opposite to the behavior of the size effect under quasi-static loading. In addition, the dynamic size effect indicates that the gap in dynamic compressive strength for specimens of different dimensions tends to be less significant under relatively low impact loading. As concluded in Ref. [14], a larger specimen corresponds to a more significant strain-rate effect on the dynamic compressive strength. The basic relationship between the strain-rate sensitivity and size dependence of the RCC is generally similar to previous testing results on all types of concrete and rocks, although this rule is accompanied by severe variability.

From the viewpoint of structural hierarchy, the weakest link of hardened RCC structure is the ITZ, where micro-cracks first initiate [24,43]. For a concrete-like material, the structural effect, always existing under impact loading, decreases the crack propagation speed due to the multiaxial stress state. Therefore, cracks need more time to completely fracture the specimens at higher strain rates, leading to a higher strength [14,29,30]. To sum up, the dynamic size effect of RCC arises from the coupled effects of the complex micro-structural hierarchy, Poisson's effect and finite crack propagation speed.

5. Modified Weibull size effect law

Most statistical analysis of brittle fracture is based on the weakest-link assumption, which is a well-accepted method to analyze the variability of concrete strength. The static size effect of concrete based on the weakest-link assumption can be illustrated as follows:

$$P(\sigma) = 1 - \exp\left[-\int_V \left(\frac{\sigma - \sigma_{th}}{\sigma_1}\right)^m \frac{dV}{V_0}\right] (\sigma \geqslant \sigma_{th}) \tag{13}$$

where P is the cumulative probability of the failure of a specimen with volume V; dV is the differential volume; V_0 is a constant representing the average volume of each microcrack; σ_{th} and σ_1 denote the threshold strength and scale parameter, respectively; and m is the shape parameter or Weibull modulus. Then, the cumulative probability P is normalized for $\sigma_{th} \leqslant \sigma \leqslant \infty$. In addition, the corresponding probability density function (p) concerning the fracture strength (σ) can be derived as follows:

$$p(\sigma) = \frac{V}{V_0} \frac{m}{\sigma_1} \left(\frac{\sigma - \sigma_{th}}{\sigma_1}\right)^{m-1} \exp\left[-\frac{V}{V_0}\left(\frac{\sigma - \sigma_{th}}{\sigma_1}\right)^m\right] (\sigma \geqslant \sigma_{th}) \tag{14}$$

From the safety viewpoint, σ_{th} can be set to zero [3]; then, the Weibull size effect law is simplified into a two-parameter form as shown in Eqs. (15) and (16).

$$P(\sigma) = 1 - \exp\left[-\frac{V}{V_0}\left(\frac{\sigma}{\sigma_1}\right)^m\right] (\sigma \geqslant 0) \tag{15}$$

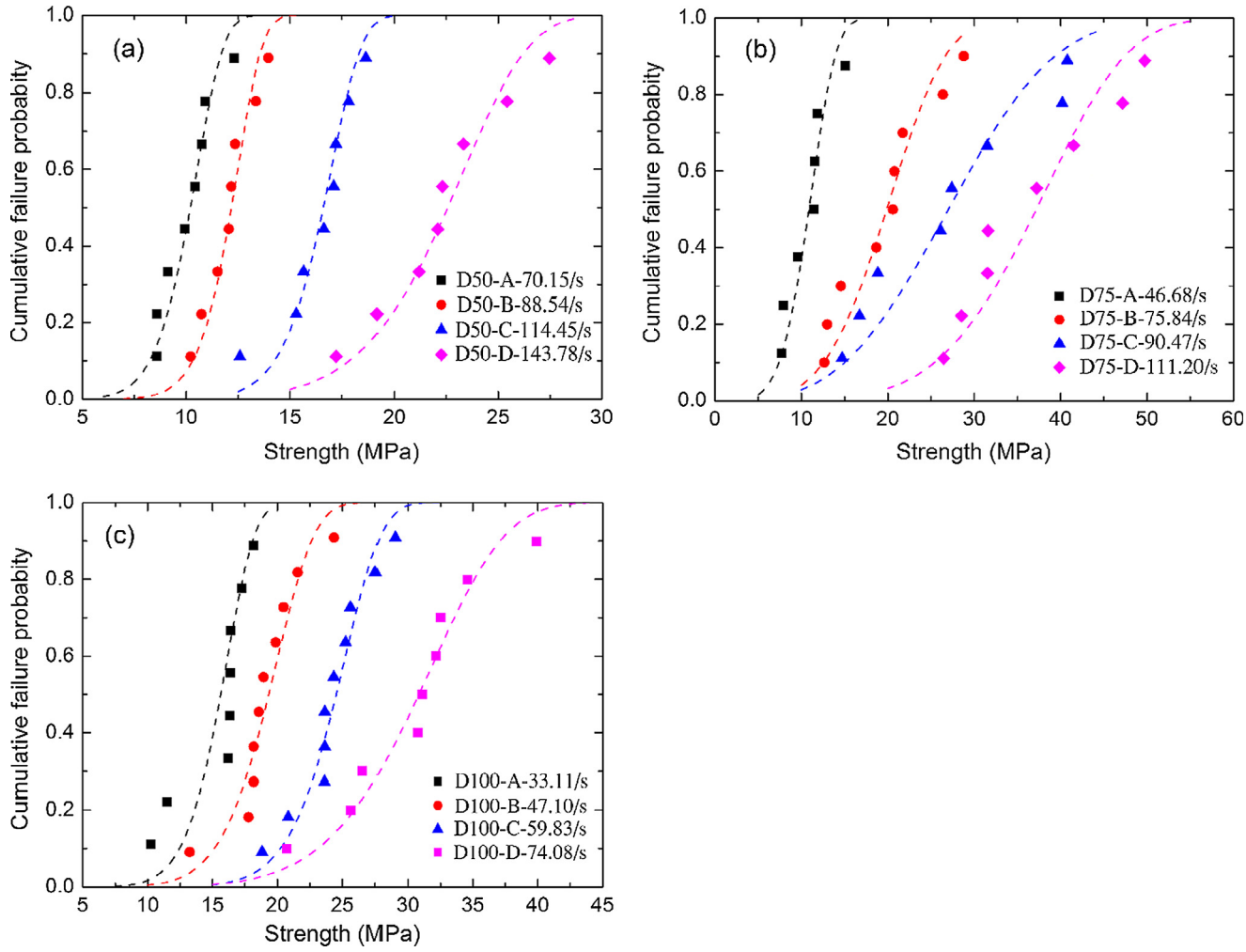

Fig. 8. CDFs of the dynamic compressive strength for specimens with various diameters: (a) D50; (b) D75; and (c) D100.

Table 5
Statistical Weibull parameters for specimens of various dimensions.

Specimen dimensions (D × L: mm × mm)	Statistical parameters					
	Group	$\dot{\varepsilon}$ (/s)	σ_0 (MPa)	m	$\bar{\sigma}$ (MPa)	s (MPa)
50 × 25	D50-A	70.15	10.63	8.79	10.06	1.37
	D50-B	88.54	12.58	11.37	12.03	1.28
	D50-C	114.45	17.11	12.39	16.42	1.61
	D50-D	143.78	23.62	8.06	22.25	3.28
75 × 25	D75-A	46.68	11.71	4.88	10.74	2.51
	D75-B	75.84	21.72	4.10	19.71	5.41
	D75-C	90.47	30.29	3.20	27.13	9.31
	D75-D	111.20	40.03	4.95	36.73	8.49
100 × 25	D100-A	33.11	16.34	8.28	15.41	2.21
	D100-B	47.10	20.28	7.69	19.06	2.93
	D100-C	59.83	25.46	9.81	24.20	2.96
	D100-D	74.08	32.62	6.51	30.40	5.46

$$p(\sigma) = \frac{V}{V_0}\frac{m}{\sigma_1}\left(\frac{\sigma}{\sigma_1}\right)^{m-1}\exp\left[-\frac{V}{V_0}\left(\frac{\sigma}{\sigma_1}\right)^{m}\right](\sigma \geqslant 0) \tag{16}$$

Many researchers have performed refined research on the size effect on the dynamic compressive strength of concrete-like materials. Notably, larger specimens are associated with a greater strain-rate sensitivity of the dynamic strength [14,15,29,30]. This phenomenon is also applicable to RCC materials, in which the dynamic strength also increases with increasing specimen size, a result that is diametrically opposed to the size effect under quasi-static loading. Thus, the static Weibull size effect law has a substantial limitation because it does not incorporate the strain rate. Considering the underlying relationship between the strain rate and specimen size, a modified size effect law is introduced, as shown in Eqs. (17) and (18).

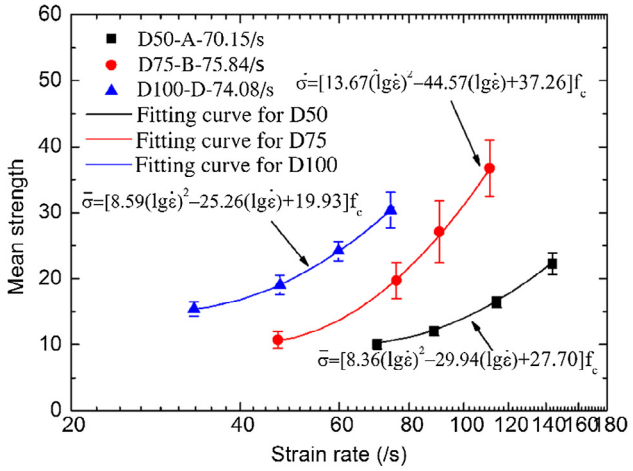

Fig. 9. Strain-rate effect on the dynamic strength using Weibull analysis.

$$P(\sigma) = 1 - \exp\left[-\left(\frac{V}{V_0}\right)^{\alpha \ln(\dot{\varepsilon}_0/\dot{\varepsilon})}\left(\frac{\sigma}{\sigma_1}\right)^m\right](\sigma \geqslant 0) \tag{17}$$

$$p(\sigma) = \left(\frac{V}{V_0}\right)^{\alpha \ln(\dot{\varepsilon}_0/\dot{\varepsilon})}\frac{m}{\sigma_1}\left(\frac{\sigma}{\sigma_1}\right)^{m-1}\exp\left[-\left(\frac{V}{V_0}\right)^{\alpha \ln(\dot{\varepsilon}_0/\dot{\varepsilon})}\left(\frac{\sigma}{\sigma_1}\right)^m\right](\sigma \geqslant 0) \tag{18}$$

where $\dot{\varepsilon}_0$ is the critical strain rate, below which the static size effect dominates. $\dot{\varepsilon}$ is the strain rate, and α is the correction factor of the strain-rate effect.

Eq. (17) can be rewritten as a logarithmic linear relation, as shown in Eq. (19). Compared to Eq. (6), the modified Weibull size law in the linear form can be seen as a modified two-parameter Weibull distribution to statistically analyze the dynamic strength of concrete material considering the size and strain-rate effects. In Ref. [44], a similar modified Weibull distribution for the dynamic strength of concrete was verified to be valid through SHPB testing at various strain rates without considering the size effect.

$$\ln[-\ln(1-P)] = \alpha(\ln V_0 - \ln V)(\ln \dot{\varepsilon} - \ln \dot{\varepsilon}_0) + m(\ln \sigma - \ln \sigma_1) \tag{19}$$

The strength is related to the specimen size and strain rate according to the proposed Weibull size effect law. Derived from Eq. (18) using the moment method, the mean value $\bar{\sigma}$ and standard deviation s can be obtained using Eqs. (20) and (21), respectively. Then, the average strength increases for larger specimens when $\dot{\varepsilon} > \dot{\varepsilon}_0$; the size effect disappears at the critical strain rate; and the average strength decreases with increasing specimen size when $\dot{\varepsilon} < \dot{\varepsilon}_0$. In addition, the size effect is enhanced at a higher strain rate, as is the standard deviation.

$$\bar{\sigma} = \sigma_1\left(\frac{V}{V_0}\right)^{\frac{\alpha}{m}\ln(\dot{\varepsilon}/\dot{\varepsilon}_0)}\Gamma\left(1+\frac{1}{m}\right) \tag{20}$$

$$s = \sigma_1\left(\frac{V}{V_0}\right)^{\frac{\alpha}{m}\ln(\dot{\varepsilon}/\dot{\varepsilon}_0)}\sqrt{\Gamma\left(1+\frac{2}{m}\right) - \Gamma^2\left(1+\frac{1}{m}\right)} \tag{21}$$

Based on the statistical results of the experimental data in Table 5, the scaling value σ_0 increases with increasing strain rate for same-size specimens. Comparing the mean and standard deviation of strength derived from the proposed Weibull size effect law in Eqs. (20) and (21) to those derived from Weibull statistics as Eqs. (7) and (8), we find that σ_0 includes the coupling effect of the strain rate and specimen size, as illustrated in Eqs. (22) and (23). Here, σ_1 becomes a constant, and shares no relationship with the specimen size and strain rate.

$$\sigma_0 = \sigma_1\left(\frac{V}{V_0}\right)^{\frac{\alpha}{m}\ln(\dot{\varepsilon}/\dot{\varepsilon}_0)} \tag{22}$$

$$\ln \sigma_0 = \ln \sigma_1 + \frac{\alpha}{m}(\ln \dot{\varepsilon} - \ln \dot{\varepsilon}_0)(\ln V - \ln V_0) \tag{23}$$

The parameter estimation has been the primary issue to verify the practicability of the proposed effect law. The shape parameter m is insensitive to the strain rate and uncoupled to the specimen size. Here, we select the mean value of the shape parameter (m = 7.50) according to Table 5, and the critical strain rate can be obtained as 40/s from Ref. [31].

Several methods are available to determine the parameter of the modified Weibull size effect law from a set of experimental strength data, in which the most widely used method is the least-squares method (LSM) analysis. Using the statistical results from the experimental data in Table 5, a linear least-squares regression analysis can be performed on Eq. (24) to determine the parameters in the proposed size effect law. As a complement,

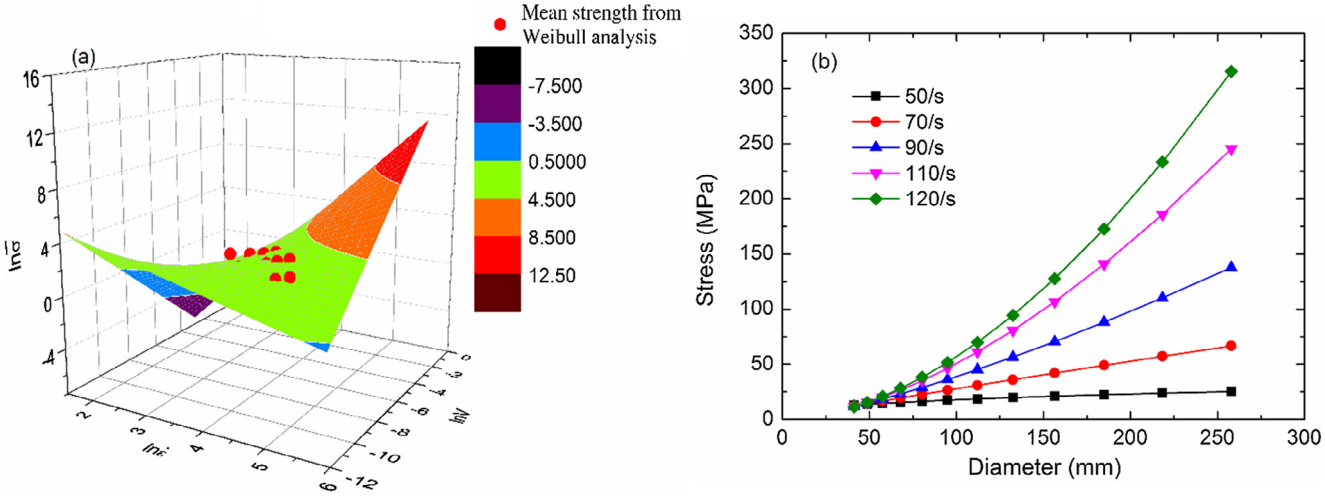

Fig. 10. Relationship of $\ln \bar{\sigma}$, $\ln V$ and $\ln \dot{\varepsilon}$: (a) size effect law in the full strain-rate scale; (b) dynamic effect law.

the volume of a specimen can be calculated as $V = \pi D^3/8$, where D is the diameter of the specimen.

$$\ln \bar{\sigma} = \ln\left[\sigma_1 \Gamma\left(1+\frac{1}{m}\right)\right] + \frac{\alpha}{m}(\ln V - \ln V_0)(\ln \dot{\varepsilon} - \ln \dot{\varepsilon}_0) \quad (24)$$

The results of parameter estimation with the experimental data from 101 successful SHPB tests are $\sigma_1 = 14.16$ MPa, $\alpha = 4.12$ and $V_0 = 3.54 \times 10^{-5}$ m^3. By substituting the fitting parameters into Eq. (24), the modified Weibull size effect law is graphically shown in Fig. 10. As an objective of this study, the strength from proposed Weibull size effect law is an estimated mean strength essentially (Eq. (24)) based on the concept of the weakest-link assumption and has an inherent relationship with the results of the Weibull analysis. In this study, the mean strength for each group has been estimated based on the Weibull analysis, as listed in Table 5. Therefore, it is necessary to compare the mean dynamic strength from Weibull analysis (Table 5) with that from proposed Weibull size effect law (Eq. (24)).

Fig. 10a shows that the experimental mean strength points from Weibull analysis are consistent with the theoretical surface of the modified size effect law. The modified size effect law can also present the basic rules that the dynamic compressive strength increases with increasing specimen size under impact loading, as shown in Fig. 10b, which is diametrically opposed to the common size effect under quasi-static loading. Moreover, the enhancement of dynamic strength becomes more sensitive to the strain rate for larger specimens.

6. Conclusions

Focusing on the dynamic size effect of the RCC material, SHPB tests on 101 cylindrical specimens with the diameters of 50 mm, 75 mm and 100 mm was conducted under high strain rate loading in this study. The dynamic size effect of the RCC material was investigated based on the experimental results within a wide range of strain rates and was reconfirmed based on ANOVA and Weibull analysis. A modified Weibull size effect law was proposed to illustrate the underlying mechanism of the dynamic size effect for the RCC material under impact loading. The main contributions and findings are as follows:

(1) The observed dynamic mechanical properties of RCC material were size dependent. The dynamic size effect under impact loading is notably different from the well-known static size effect, in which the dynamic mechanical properties, e.g., the peak strength, ultimate strain and toughness, increases with the increasing sample size at a similar strain rate.
(2) Besides contributions from material heterogeneity, the dynamic size effect partly consists of contributions from lateral inertial confinement due to strain rate effect, which is significantly important for larger specimens. A larger specimen corresponds to a more prominent strain-rate effect on the dynamic compressive strength, i.e., the experimental peak strength for larger specimens is more sensitive to the strain rate.
(3) More significant scatter of the stress-strain curves and DIFs was directly observed from the dynamic compressive tests at higher strain rates. The Weibull analysis also showed that the variance of dynamic compressive strength for RCC specimens tended to be larger under higher impact loading. Therefore, more attentions should be paid to the variance of dynamic compressive strength from material heterogeneity in structural dynamic analysis, considering the dynamic size effect.
(4) A modified size effect law considering the strain-rate effect was proposed to illustrate the underlying mechanism of the size effect for the RCC material. The proposed size effect law can be formulated as a modified two-parameter Weibull distribution to statistically analyze the strength of the concrete material, considering the strain rate and specimen size. Finally, the relationships of the material strength, specimen size and strain rate were further described under a unified theoretical framework containing static and dynamic loading.

Acknowledgment

This research was supported by the National Natural Science Foundation of China (grant nos. 51509182 and 51679168).

References

[1] W.S. Lei, Z. Yu, A statistical approach to scaling size effect on strength of concrete incorporating spatial distribution of flaws, Constr. Build. Mater. 122 (2016) 702–713, https://doi.org/10.1016/j.conbuildmat.2016.06.102.
[2] H.K. Man, J.G.M.V. Mier, Damage distribution and size effect in numerical concrete from lattice analyses, Cem. Concr. Compos. 33 (2011) 867–880, https://doi.org/10.1016/j.cemconcomp.2011.01.008.
[3] Z.P. Bažant, M. Vovrechovský, D. Novak, Asymptotic prediction of energetic-statistical size effect from deterministic finite element solutions, J. Eng. Mech. 133 (2007) 153–162, https://doi.org/10.1061/(ASCE)0733-9399(2007) 133:2 (153).
[4] C.G. Hoover, Z.P. Bažant, Cohesive crack, size effect, crack band and work-of-fracture models compared to comprehensive concrete fracture tests, Int. J. Fract. 187 (2014) 133–143, https://doi.org/10.1007/s10704-013-9926-0.
[5] Z.P. Bažant, Probability distribution of energetic-statistical size effect in quasibrittle fracture, Probabilist. Eng. Mech. 19 (2004) 307–319, https://doi.org/10.1016/j.probengmech.2003.09.003.
[6] S. Morel, Size effect in quasibrittle fracture: derivation of the energetic size effect law from equivalent LEFM and asymptotic analysis, Int. J. Fract. 154 (2008) 15–26, https://doi.org/10.1007/s10704-008-9291-6.
[7] A. Carpinteri, S. Puzzi, A fractal approach to indentation size effect, Eng. Fract. Mech. 73 (2006) 2110–2122, https://doi.org/10.1016/j.engfracmech.2006.04.020.
[8] J. Xiao, L. Li, L. Shen, S.P. Chi, Compressive behaviour of recycled aggregate concrete under impact loading, Cem. Concr. Res. 71 (2015) 46–55, https://doi.org/10.1016/j.cemconres.2015.01.014.
[9] T.J. Holmquist, G.R. Johnson, W.H. Cook, A computational constitutive model for concrete subjected to large strains, high strain rates, and high pressures, in: Proceedings, 14th Int. Symp. Ballist., Quebec, Canada, 1993, pp. 591–600.
[10] H. Hao, Y. Hao, J. Li, W. Chen, Review of the current practices in blast-resistant analysis and design of concrete structures, Adv. Struct. Eng. 19 (2016) 1193–1223, https://doi.org/10.1177/1369433216656430.
[11] W. Ren, J. Xu, H. Su, Dynamic compressive behaviour of concrete after exposure to elevated temperatures, Mater. Struct. 49 (2016) 3321–3334, https://doi.org/10.1617/s11527-015-0722-3.
[12] M. Xu, K. Wille, Fracture energy of UHP-FRC under direct tensile loading applied at low strain rates, Compos. Part B 80 (2015) 116–125, https://doi.org/10.1016/j.compositesb.2015.05.031.
[13] M.M. Elfahal, T. Krauthammer, T. Ohno, M. Beppu, S. Mindess, Size effect for normal strength concrete cylinders subjected to axial impact, Int. J. Impact Eng. 31 (2005) 461–481, https://doi.org/10.1016/j.ijimpeng.2004.01.003.
[14] C. Qi, M. Wang, J. Bai, K. Li, Mechanism underlying dynamic size effect on rock mass strength, Int. J. Impact Eng. 68 (2014) 1–7, https://doi.org/10.1016/j.ijimpeng.2014.01.005.
[15] Y. Hao, H. Hao, G.P. Jiang, Y. Zhou, Experimental confirmation of some factors influencing dynamic concrete compressive strengths in high-speed impact tests, Cem. Concr. Res. 52 (2013) 63–70, https://doi.org/10.1016/j.cemconres.2013.05.008.
[16] Y. Hao, H. Hao, Z.X. Li, Influence of end friction confinement on impact tests of concrete material at high strain rate, Int. J. Impact Eng. 60 (2013) 82–106, https://doi.org/10.1016/j.ijimpeng.2013.04.008.
[17] Y. Hao, H. Hao, Z.X. Li, Numerical analysis of lateral inertial confinement effects on impact test of concrete compressive material properties, Int. J. Prot. Struct. 1 (2010) 145–168, https://doi.org/10.1260/2041-4196.1.1.145.
[18] M.R.A.V. Vliet, J.G.M.V. Mier, Effect of strain gradients on the size effect of concrete in uniaxial tension, Int. J. Fract. 95 (1999) 195–219, https://doi.org/10.1023/A:1018652302261.
[19] M.R.A.V. Vliet, J.G.M.V. Mier, Experimental investigation of size effect in concrete and sandstone under uniaxial tension, Eng. Fract. Mech. 65 (2000) 165–188, https://doi.org/10.1016/S0013-7944(99)00114-9.

[20] Q.M. Li, H. Meng, About the dynamic strength enhancement of concrete-like materials in a split Hopkinson pressure bar test, Int. J. Solids Struct. 40 (2003) 343–360, https://doi.org/10.1016/S0020-7683(02)00526-7.
[21] Q.M. Li, Y.B. Lu, H. Meng, Further investigation on the dynamic compressive strength enhancement of concrete-like materials based on split Hopkinson pressure bar tests. Part II: Numerical simulations, Int. J. Impact Eng. 36 (2009) 1335–1345, https://doi.org/10.1016/j.ijimpeng.2009.04.010.
[22] Y. Hao, H. Hao, Numerical evaluation of the influence of aggregates on concrete compressive strength at high strain rate, Int. J. Prot. Struct. 2 (2011) 177–206, https://doi.org/10.1260/2041-4196.2.2.177.
[23] Y. Su, J. Li, C. Wu, P. Wu, Z.X. Li, Influences of nano-particles on dynamic strength of ultra-high performance concrete, Compos. Part B 91 (2016) 595–609, https://doi.org/10.1016/j.compositesb.2016.01.044.
[24] G. Chen, Y. Hao, H. Hao, 3D meso-scale modelling of concrete material in spall tests, Mater. Struct. 48 (6) (2014) 1887–1899, https://doi.org/10.1617/s11527-014-0281-z.
[25] X. Wang, Z. Yang, A.P. Jivkov, Monte Carlo simulations of mesoscale fracture of concrete with random aggregates and pores: a size effect study, Constr. Build. Mater. 80 (2015) 262–272, https://doi.org/10.1016/j.conbuildmat.2015.02.002.
[26] J.G.M.V. Mier, M.R.A.V. Vliet, Influence of microstructure of concrete on size/scale effects in tensile fracture, Eng. Fract. Mech. 70 (2003) 2281–2306, https://doi.org/10.1016/S0013-7944(02)00222-9.
[27] M.M.R. Taha, A.S. El-Dieb, M.A.A. El-Wahab, M.E. Abdel-Hameed, Mechanical, fracture, and microstructural investigations of rubber concrete, J. Mater. Civ. Eng. 20 (2008) 640–649, https://doi.org/10.1061/(ASCE)0899-1561(2008)20:10(640).
[28] J.E.A. Flores, Q.M. Li, Structural effects on compressive strength enhancement of concrete-like materials in a split Hopkinson pressure bar test, Int. J. Impact Eng. 109 (2017) 408–418, https://doi.org/10.1016/j.ijimpeng.2017.08.003.
[29] C. Qi, M. Wang, J. Bai, X. Wei, H. Wang, Investigation into size and strain rate effects on the strength of rock-like materials, Int. J. Rock Mech. Min. 86 (2016) 132–140, https://doi.org/10.1016/j.ijrmms.2016.04.008.
[30] C. Qi, M. Wang, Q. Qian, Strain-rate effects on the strength and fragmentation size of rocks, Int. J. Impact Eng. 36 (2009) 1355–1364, https://doi.org/10.1016/j.ijimpeng.2009.04.008.
[31] S.R. Zhang, X.H. Wang, C. Wang, R. Song, H.Y. Huo, Compressive behavior and constitutive model for roller compacted concrete under impact loading: considering vertical stratification, Constr. Build. Mater. 151 (2017) 428–440, https://doi.org/10.1016/j.conbuildmat.2017.06.113.
[32] Q.S. Li, J.Q. Fang, D.K. Liu, J. Tang, Failure probability prediction of concrete components, Cem. Concr. Res. 33 (2003) 1631–1636, https://doi.org/10.1016/S0008-8846(03)00111-X.
[33] National Energy Administration, Code for Mix Design of Hydraulic Concrete (DL/T5330-2015), China Electric Power Press, Beijing, 2015 (in Chinese).
[34] F. Saint-Pierre, A. Philibert, B. Giroux, P. Rivard, Concrete quality designation based on ultrasonic pulse velocity, Constr. Build. Mater. 125 (2016) 1022–1027, https://doi.org/10.1016/j.conbuildmat.2016.08.158.
[35] X. Chen, S. Wu, J. Zhou, Experimental and modeling study of dynamic mechanical properties of cement paste, mortar and concrete, Constr. Build. Mater. 47 (2013) 419–430, https://doi.org/10.1016/j.conbuildmat.2013.05.063.
[36] D.L. Grote, S.W. Park, M. Zhou, Dynamic behavior of concrete at high strain rates and pressures: I. Experimental characterization, Int. J. Impact Eng. 25 (2001) 869–886, https://doi.org/10.1016/S0734-743X(01)00020-3.
[37] W. Riedel, K. Thoma, S. Hiermaier, E. Schmolinske, Penetration of reinforced concrete by BETA-B-500 numerical analysis using a new macroscopic concrete model for hydrocodes, in: Proceedings, 9th Int. Symp. Eff. Munitions with Struct., Berlin, Germany, 1999, pp. 1–8.
[38] P.H. Bischoff, S.H. Perry, Compressive behaviour of concrete at high strain rates, Mater. Struct. 24 (1991) 425–450, https://doi.org/10.1007/BF02472016.
[39] Y. Hao, H. Hao, Influence of the concrete DIF model on the numerical predictions of RC wall responses to blast loadings, Eng. Struct. 73 (2014) 24–38, https://doi.org/10.1016/j.engstruct.2014.04.042.
[40] H. Hao, X. Zhou, Concrete material model for high rate dynamic analysis, Proceedings, 7th Int. Conf. Shock Impact Loads Struct., Beijing, China, 2007.
[41] A. Chatterjee, D. Das, Taguchi and ANOVA approach for optimization of flow characteristics of self-compacting concrete, J. Virol. 3 (2013) 37–45, https://doi.org/10.1680/emr.13.00016.
[42] Z.P. Bažant, Mechanics based statistical prediction of structure size and geometry effects on safety factors for composites and other quasibrittle materials, Theor. Appl. Mech. 35 (2008) 53–71, https://doi.org/10.2514/6.2007-1972.
[43] T. Akçaoğlu, M. Tokyay, T. Çelik, Effect of coarse aggregate size and matrix quality on ITZ and failure behavior of concrete under uniaxial compression, Cem. Concr. Compos. 26 (2004) 633–638, https://doi.org/10.1016/s0958-9465(03)00092-1.
[44] X. Chen, S. Wu, J. Zhou, Compressive strength of concrete cores under high strain rates, J. Perform. Constr. Facil. 29 (2015) 06014005, https://doi.org/10.1061/(asce)cf.1943-5509.0000586.